

## Electron signals from heavy-lepton cascade decays\*

Carl H. Albright

Department of Physics, Northern Illinois University, DeKalb, Illinois 60115<sup>†</sup>  
and Fermi National Accelerator Laboratory,<sup>‡</sup> Batavia, Illinois 60510

J. Smith and J. A. M. Vermaseren

Institute for Theoretical Physics, State University of New York at Stony Brook, Stony Brook, New York 11794

(Received 16 June 1977)

The heavy-lepton-cascade interpretation of neutrino-induced multimMuon events also yields events with electrons which can be identified in bubble-chamber experiments. We study processes giving rise to single-electron events, dilepton  $\mu^-e^+, \mu^-e^-$  events, and trilepton  $\mu\mu e, \mu ee$  events. Rates are presented for different quark transitions. We give results for distributions and also discuss the background reaction  $\nu_e + N \rightarrow e^- + X$  caused by contamination of the muon-type neutrino beam by electron-type neutrinos.

### I. INTRODUCTION

The observations of neutrino-induced trimuon events in the Caltech-Fermilab (CF),<sup>1</sup> Fermilab-Harvard-Pennsylvania-Rutgers-Wisconsin (FHPRW),<sup>2</sup> and CERN-Dortmund-Heidelberg-Saclay (CDHS)<sup>3</sup> counter experiments at Fermilab and CERN have prompted numerous speculations concerning the origin(s) of these events. One of the viable explanations, namely the production and subsequent cascade decay of heavy leptons, has been studied at some length by the present authors<sup>4</sup> and independently by Barger *et al.*,<sup>5</sup> who calculated distributions in good accord with the experimental findings. The relatively high event rate can be understood in models which are based on gauge groups<sup>6</sup> larger than the standard Weinberg-Salam model, such as  $SU(3) \otimes U(1)$  or  $SU(2) \otimes SU(2) \otimes U(1)$ . This interpretation allows a simple extension to semileptonic modes to explain the same-sign dimuon events. The opposite-sign dimuon events,<sup>7</sup> on the other hand, arise primarily from the decay of singly produced charmed particles.<sup>8</sup>

Other possible explanations for the trimuon events have been proposed: associated production of charm in the parton model with each charmed particle decaying semileptonically into muons;<sup>9</sup> diffractive production of a pair of charmed particles followed by their semileptonic decay;<sup>10</sup> or production of a heavy neutral  $M^0$  lepton in association with a  $d \rightarrow b$  quark transition at the hadronic vertex with the bottom flavored hadron decaying semileptonically into a muon and with the  $M^0$  decaying leptonically into a muon pair and a neutrino.<sup>11</sup>

One would like to test these ideas further by comparing dilepton  $\mu e$  events and trilepton  $\mu\mu e$  and  $\mu ee$  events with the predictions of these models. Neutrino- and antineutrino-induced  $\mu e$

events have been observed in bubble chambers by the CERN Gargamelle group,<sup>12</sup> and by groups at Brookhaven<sup>13</sup> and Argonne,<sup>13</sup> as well as by the Fermilab-IHEP-ITEP-Michigan (FIIM),<sup>14</sup> Wisconsin-Berkeley-CERN-Hawaii,<sup>15</sup> and Columbia-Brookhaven-Fermilab (CBF)<sup>16</sup> collaborations at Fermilab, but no trilepton candidates have been seen to date. Unlike the same-sign dimuon and trimuon events, observation of both muons and electrons allows one to distinguish leptons emitted at the different vertices in the chain decays. In this paper we shall focus our attention primarily on distributions for the lepton-cascade model, but make comments where appropriate regarding the other models.

If the heavy-lepton-cascade interpretation proves to be inherently correct, it will be of special interest to test for the presence of neutral-current (flavor-changing) couplings as well as the charged-current ones. Also, the question must be settled whether the quark transition at the hadron vertex is of the light-to-light or light-to-heavy quark variety. This can be determined by studying the energy distributions for the emitted hadrons and leptons as well as the visible energy distributions for a given neutrino beam configuration. If only light-to-heavy quark transitions can take place at the hadron vertex, the observed distributions will exhibit delayed threshold features.<sup>4</sup>

In what follows, we shall first investigate in Sec. II the production process  $\nu_\mu + N \rightarrow M^- + X$  for a (5–8)-GeV/ $c^2$  heavy lepton. For this purpose we shall fold the production cross section with the 400-GeV double-horn spectra used by the CBF collaboration at Fermilab since this group has by far the greatest statistics on the  $\mu e$  events. We then compare predictions for single-electron events arising from the decay  $M^- \rightarrow \nu_\mu + e^- + \bar{\nu}_e$  with those for  $\nu_e + N \rightarrow e^- + X$  events arising from the  $\nu_e$  background component in the  $\nu_\mu$  beam.

In Sec. III we study briefly opposite-sign dilepton processes yielding  $\mu^-e^+$ . These are identical to the  $\mu^-\mu^+$  results in Ref. 4, except for the different neutrino spectrum used in the flux-averaging. In Sec. IV the  $\mu^-e^-$  results are presented in more detail, since the identity problem does not exist here as was the case for the  $\mu^-\mu^-$  events. Reactions giving rise to trilepton events are studied in Sec. V, and our conclusions are given in Sec. VI.

## II. SINGLE-ELECTRON PROCESSES

Our starting point is the production process

$$\nu_\mu + N \rightarrow M^- + X \quad (2.1a)$$

and its counterpart

$$\bar{\nu}_\mu + N \rightarrow M^+ + X, \quad (2.1b)$$

for which cross-section curves were presented in our previous work<sup>4</sup> in several phenomenological

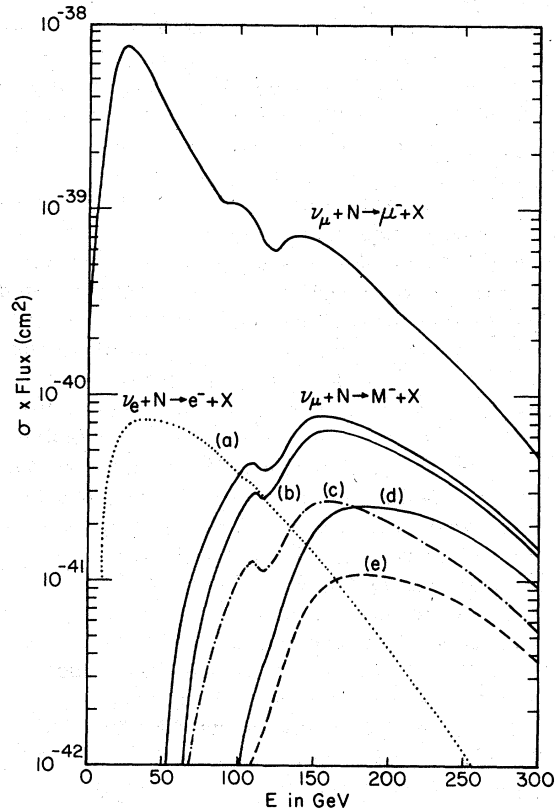


FIG. 1. Total-cross-section-times-flux curves for  $e^-$ ,  $\mu^-$ , and  $M^-$  production by neutrinos from the double horn. The curves (a), (b), (c), (d), and (e) refer to  $M^-$  production together with light quarks ( $V-A$  coupling), charmed quarks ( $V-A$  coupling), ( $V+A$  coupling), and heavy quarks ( $V-A$  coupling) ( $V+A$  coupling), respectively.

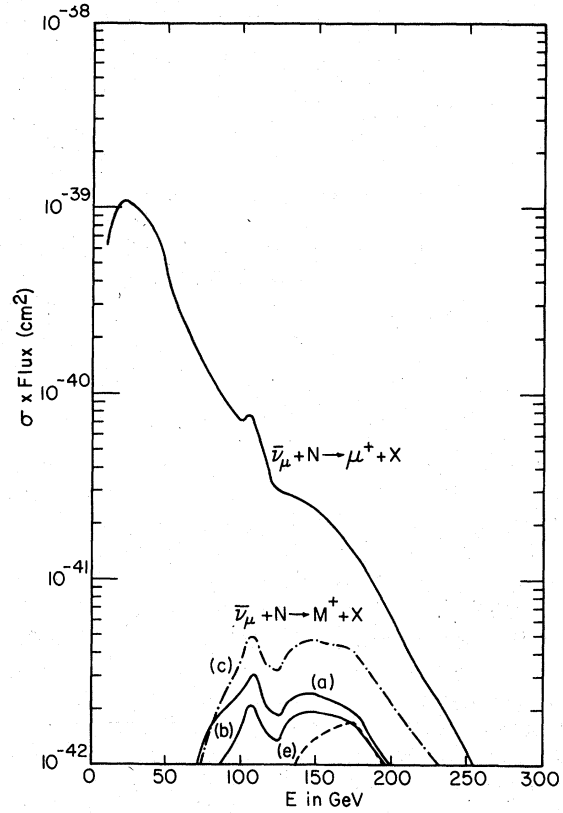


FIG. 2. Same as Fig. 1 using antineutrinos from the double horn with plug.

models involving light-to-light and light-to-heavy quark transitions with both  $V-A$  and  $V+A$  currents. It is of interest to fold in the neutrino spectra for the focusing-horn beams used in the bubble-chamber experiments so as to compare the event rate curves directly with those presented in Figs. 6 and 8 of Ref. 4 for the quadrupole-triplet  $\nu$  (and  $\bar{\nu}$ ) beam used by the FHPRW counter group. In Fig. 1 we give the energy dependence of  $\sigma \times \text{flux}$  for the double-horn setup used by the CBF neutrino group, while in Fig. 2 we give the predicted production rates for the double-horn-with-plug setup used by the FIIM antineutrino group. As in Ref. 4, the heavy-lepton production curves apply for a heavy lepton of mass  $8 \text{ GeV}/c^2$  and are labeled according to the convention introduced there. Curve (a) refers to a full-strength  $V-A$  interaction which couples  $d$  to  $u$  quarks through the conventional  $W^+$  field. Curves (b) and (c) refer to  $V-A$ ,  $V+A$  coupling of  $d$  to  $c$  quarks with quark mass  $m_c = 1.5 \text{ GeV}/c^2$  and physical threshold mass  $M_c = 2.25 \text{ GeV}/c^2$ . Curves (d) and (e) refer to  $V-A$ ,  $V+A$  coupling of  $d$  to  $t$  quarks with quark and physical threshold masses of  $m_t = 4 \text{ GeV}/c^2$  and  $M_t = 5 \text{ GeV}/c^2$ , re-

TABLE I. Flux-averaged cross-section ratios  $R^\nu$  and  $R^{\bar{\nu}}$ . The quark transitions are listed for the neutrino reaction. Regarding antineutrinos we chose  $u \rightarrow d$ ,  $u \rightarrow b(m_b = m_c)$ , and  $u \rightarrow b(m_b = m_t)$ , respectively.

Quark transition	Coupling type	Mass (GeV/c <sup>2</sup> )	$R^\nu$ ( $E > 10$ GeV)	$R^{\bar{\nu}}$ ( $E > 10$ GeV)
$d \rightarrow u$	$V - A$	5	0.12	0.05
		8	0.03	0.007
	$V + A$	5	0.05	0.14
		8	0.01	0.02
$d \rightarrow c$	$V - A$	5	0.10	0.04
		8	0.02	0.005
	$V + A$	5	0.04	0.09
		8	0.009	0.01
$d \rightarrow t$	$V - A$	5	0.04	0.01
		8	0.009	0.001
	$V + A$	5	0.02	0.02
		8	0.004	0.003

spectively. Also shown in Fig. 1 is the expected  $\nu_e + N \rightarrow e^- + X$  event rate arising from the  $\nu_e$  background flux in the  $\nu_\mu$  beam. For antineutrinos the quark transitions correspond to  $u \rightarrow d$ ,  $u \rightarrow b(m_b = m_c)$ , and  $u \rightarrow b(m_b = m_t)$ , respectively.

Since the horn spectra are much softer than the beams from the quadrupole-triplet target train, the secondary peaks in the single-muon inclusive channels arising from kaon neutrinos in Figs. 6 and 8 of Ref. 4 are reduced to shoulder effects in Figs. 1 and 2 (see also Ref. 5). The peak  $M^-$  event rate is at most 1% of the peak single  $\mu^-$  inclusive rate; in the antineutrino channel (2.1b), the number is even smaller,  $\sim 0.3\%$ . In contrast, with the quadrupole-triplet target train, the corresponding ratios are 5 and 2%, respectively.

In Table I we give the flux-averaged cross-section ratios

$$R^\nu = \frac{\langle \sigma(\nu_\mu + N \rightarrow M^- + X) \rangle}{\langle \sigma(\nu_\mu + N \rightarrow \mu^- + X) \rangle}, \quad (2.2a)$$

$$R^{\bar{\nu}} = \frac{\langle \sigma(\bar{\nu}_\mu + N \rightarrow M^+ + X) \rangle}{\langle \sigma(\bar{\nu}_\mu + N \rightarrow \mu^+ + X) \rangle} \quad (2.2b)$$

for the different production mechanisms involving  $d \rightarrow u$ ,  $d \rightarrow c$ , and  $d \rightarrow t$  quark transitions with both full-strength  $V - A$  and  $V + A$  couplings at the hadron vertex. We have excluded the cross section below  $E_{\text{beam}} = 10$  GeV, even though this is a small effect. Masses of 5 and 8 GeV/c<sup>2</sup> are chosen for the heavy lepton with quark and physical threshold masses as given earlier in this section. It is seen that the ratios depend sensitively upon the model chosen, as is also clear from Figs. 1 and 2. Changing the mass from 8 GeV/c<sup>2</sup> down to 5 GeV/c<sup>2</sup> enhances the ratios by a factor of 4 to 10. In any case, since the event rate for anti-

neutrino production of  $M^+$  is much suppressed by the rapidly falling  $\bar{\nu}$  flux spectrum above 100 GeV, we shall concentrate on the neutrino processes in the following.

Once produced, the  $M^-$  heavy lepton can decay into a number of different channels which are enumerated in Ref. 4. Here we are interested in the single-electron decay mode

$$M^- \rightarrow e^- + \text{neutrinos}. \quad (2.3)$$

We estimate the branching ratio for this decay mode to be in the range 10–15% depending upon the model.<sup>17</sup> It is possible, however, that this decay mode is strictly forbidden in lowest order in a gauge model where the  $(M^- \nu_\mu)$  and  $(e^- \nu_e)$  pairs cannot be coupled by the same gauge field. If (2.3) can take place, the (2.1a) production and (2.3) decay processes lead to the observed reaction

$$\nu_\mu + N \rightarrow e^- + \text{hadrons} + \text{neutrinos}, \quad (2.4)$$

which competes with associated production of charm by the neutral-current process

$$\nu_\mu + N \rightarrow \nu_\mu + X_c + X_{\bar{c}} \rightarrow \text{hadrons} \rightarrow x + e^- + \bar{\nu}_e, \quad (2.5)$$

with the  $M^0$  heavy-lepton hypothesis

$$\nu_\mu + N \rightarrow M^0 + X_L \rightarrow \nu_\mu + x \rightarrow x + e^- + \bar{\nu}_e, \quad (2.6)$$

and (more importantly) with events of the type

$$\nu_e + N \rightarrow e^- + X \quad (2.7)$$

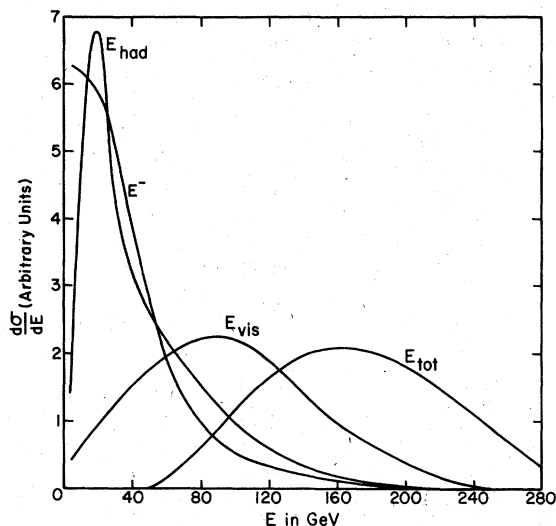


FIG. 3. Energy distributions for the  $e^-$ , the hadronic energy  $E_{\text{had}}$ , the visible  $E_{\text{vis}}$ , and the total energy  $E_{\text{tot}}$ , all flux-averaged with the neutrino spectrum. The mass of  $M^-$  is  $8 \text{ GeV}/c^2$ .

arising from the  $\nu_e$  background flux. By comparison of energy, angle,  $x$  and  $y$  distributions, one can hope to discriminate the (2.4) process from the other reactions (2.5)–(2.7). In making the comparisons, we shall include the experimental cut imposed in the CBF experiment which requires

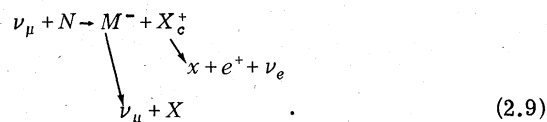
$$p_e > 1 \text{ GeV}/c, \quad (2.8)$$

and flux-average with the CBF 400-GeV double-horn spectrum (see also Ref. 5).

Before we give results of actual calculations we would like to make some estimates of the energies of the electrons produced in reactions (2.4)–(2.7). The heavy lepton in reaction (2.4) takes on the average  $\frac{2}{3}$  of the available energy when it is produced. During the decay process the energy is shared approximately equally among the decay products, so on the average the final electron receives roughly  $\frac{2}{9}$  of the average beam energy. In reaction (2.7) it is well known that the average energy of the electron is  $\frac{1}{2}$  of the average beam energy. The other reactions can be distinguished because they yield much slower electrons. In (2.5) it is unlikely that the average energy of the  $X_c$  is larger than  $\frac{1}{3}$  of the beam energy. Also, the quark (or hadron) only takes a fraction of this energy ( $\frac{1}{2}$  is a rather optimistic number which we adopt for illustration), so that the final  $e^-$  energy is only  $\lesssim \frac{1}{18}$  of the beam energy. Similarly the heavy  $M^0$  takes approximately  $\frac{2}{3}$  of the total energy leaving only  $\frac{1}{3}$  for the  $X_c$  so we again expect the final  $e^-$  energy to average around  $\frac{1}{18}$  of the

total. Hence we expect fast electrons to come from reaction (2.7) with slower electrons coming from (2.4) and finally rather slow electrons from (2.5) and (2.6).

Reaction (2.5) does not involve heavy leptons and will not be discussed further. We have examined the distributions from the neutral-current reaction (2.6), which are similar to the distributions in the analogous charged-current reaction



However, because the rate for the neutral-current reaction is expected to be smaller than the corresponding rate for reaction (2.4), we will mainly concentrate on the differences between reactions (2.4) and (2.7). A study of single-muon inclusive distributions is currently being prepared and will contain a more elaborate discussion of the differences between the models.

In Figs. 3 and 4 with a  $M^-$  mass of  $8 \text{ GeV}/c^2$  and  $5 \text{ GeV}/c^2$ , respectively, we present the energy distributions for the electron, the hadrons, the visible energy, and the true (but unmeasurable) total energy. Here we have chosen a  $d \rightarrow u$   $V-A$  current quark transition at the hadron vertex. In Fig. 5 a similar graph is presented for a  $5\text{-GeV}/c^2$   $M^-$  heavy lepton but with a  $d \rightarrow t$  quark transition with a  $V-A$  current. Changing to a  $V+A$  current at the hadron vertex alters the energy distributions very little. For comparison, in Fig. 6 we show the relevant energy distributions

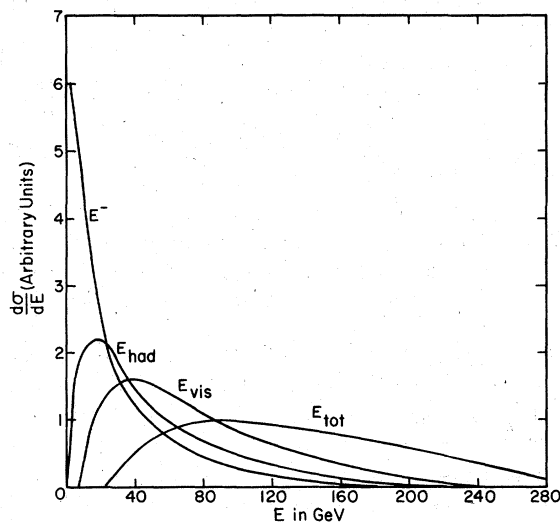


FIG. 4. Same as Fig. 3 with a  $5\text{-GeV}/c^2$   $M^-$  mass.

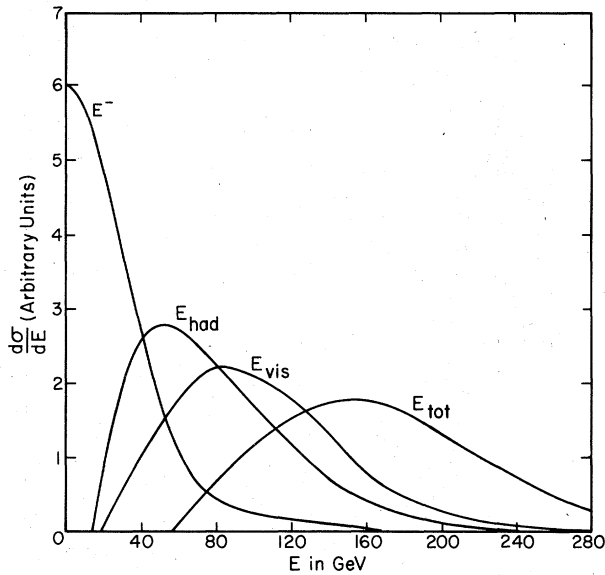


FIG. 5. Same as Fig. 3 with a  $5\text{-GeV}/c^2 M^-$  mass and a  $d \rightarrow t$  quark transition.

for the  $\nu_e$  background reaction (2.7).

The  $E_e$  distribution for an  $8 \text{ GeV}/c^2 M^-$  is considerably broader than for a  $5 \text{ GeV}/c^2 M^-$ , since more energy is available to the electron; however, for a  $5 \text{ GeV}/c^2 M^-$  produced in a reaction leading to a light-to-heavy quark transition, the  $E_e$  distribution is broadened somewhat relative to that for a light-to-light quark transition due to the larger threshold energy required for the reaction (2.1). The electron energy distribution for the  $\nu_e$

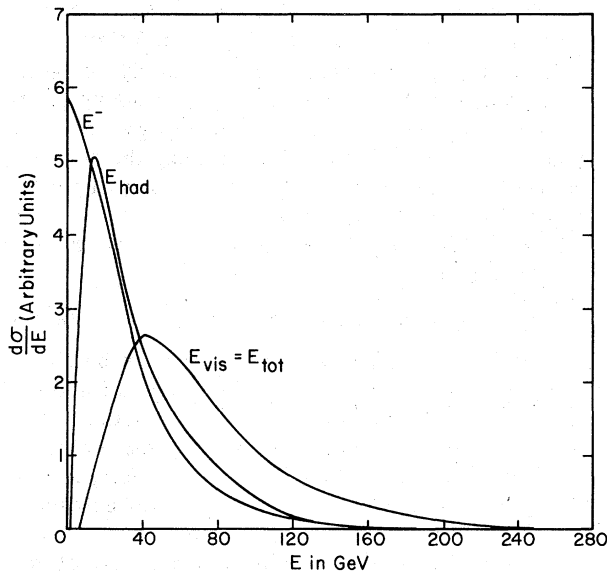


FIG. 6. Same as Fig. 3 for the background reaction  $\nu_e + N \rightarrow e^- + X$ .

reaction is most similar to that in Fig. 5.

The hadron energy distribution is peaked near 20 GeV in Figs. 3, 4, and 6 and falls most rapidly for reaction (2.7). For Fig. 5 corresponding to the  $d \rightarrow t$  transition, however, the peak occurs around 60 GeV and is noticeably broader than for the other cases considered. The visible energy distributions for the  $\nu_e$  background reaction (2.7) and for the  $5 \text{ GeV}/c^2 M^-$  in Fig. 4 peak near 40 GeV and are skewed in appearance. For the other two cases illustrated in Figs. 3 and 5, the visible energy distribution peaks near 85 GeV and is more symmetrical in shape. On the basis of the energy distributions shown, we see that a  $5 \text{ GeV}/c^2 M^-$  with  $d-u$  transition most nearly mimics the  $\nu_e$  process. The other two cases exhibit features which should stand out against those from the  $\nu_e$  background reaction.

The  $x$  distributions for the  $8 \text{ GeV}/c^2$  and  $5 \text{ GeV}/c^2 M^-$  with  $d-u$  transition,  $5 \text{ GeV}/c^2 M^-$  with  $d-t$  transition, and for the  $\nu_e$  background reaction are all shown in Fig. 7. The  $x$  distribution for reaction (2.7) has the standard form: At  $x=0$  it falls to approximately one-half its peak value; it peaks near  $x=0.25$  and falls to zero at  $x=1$ . This same scaling distribution was used as input for the structure functions in the lepton production process. The visible  $x$  distribution for the heavy-lepton chain reaction (2.4) defined

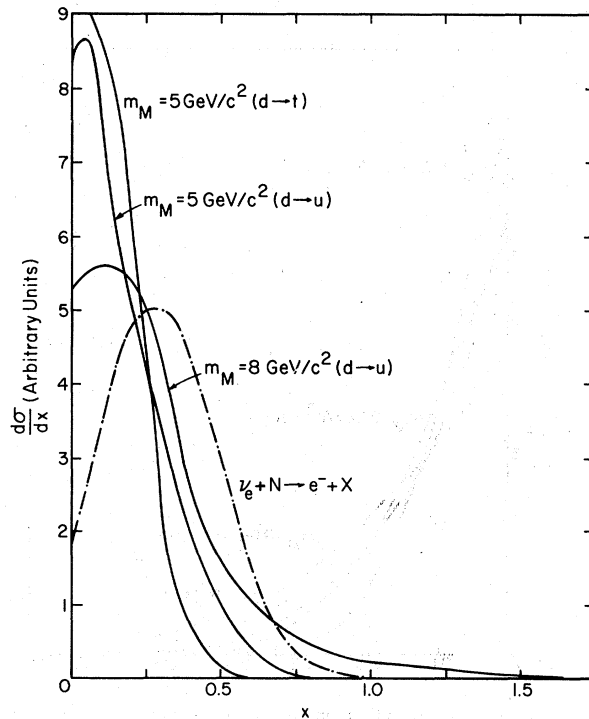


FIG. 7. The distributions in  $x_{\text{vis}}$  for reaction (2.4) (solid lines), reaction (2.7) (dot-dashed line).

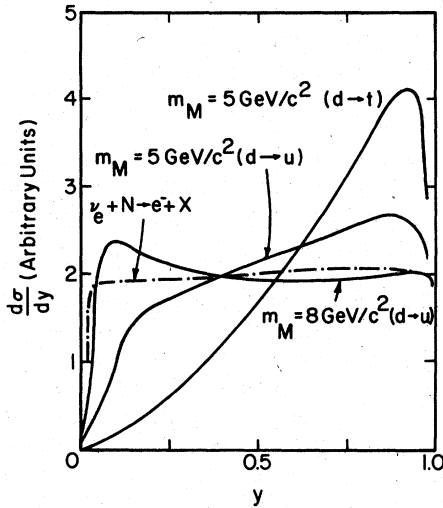


FIG. 8. The distributions in  $y_{\text{vis}}$  for reaction (2.4) (solid lines), reaction (2.7) (dot-dashed line).

by

$$\begin{aligned} x_{\text{vis}} &= q_{\text{vis}}^2 / (2ME_{\text{had}}) \\ &= E_{\text{vis}} E_e (1 - \cos\theta_e) / (ME_{\text{had}}) \end{aligned} \quad (2.10)$$

is much more sharply peaked in the small- $x$  region. The peak is narrowest for the  $5 \text{ GeV}/c^2 M^-$  with  $d \rightarrow t$  transition, and broader for the other two. In fact, for the  $8 \text{ GeV}/c^2 M^-$ , the tail extends beyond  $x = 1$ . This can arise when the ap-

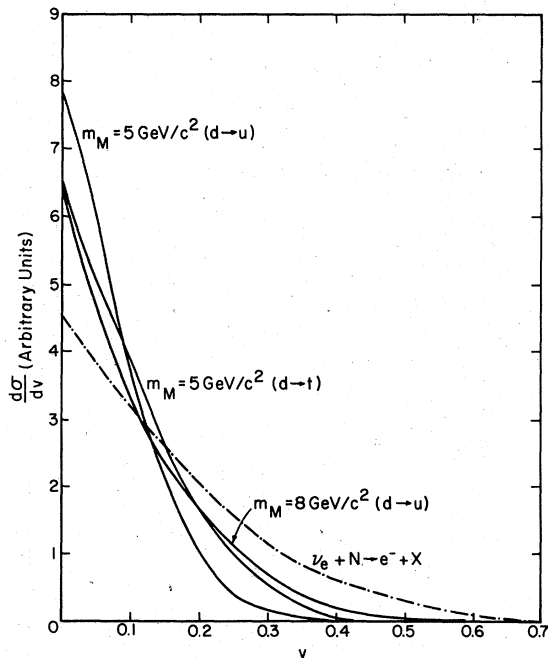


FIG. 9. The distribution in  $v_{\text{vis}}$  for reactions (2.4) and (2.7). The notation is the same as in Figs. 7 and 8.

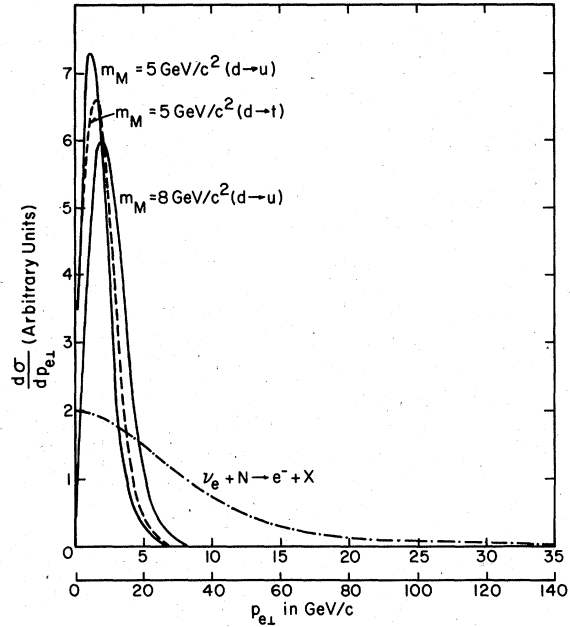


FIG. 10. The distributions in transverse momentum relative to neutrino beam.

parent  $q^2 = q_{\text{vis}}^2$  is larger than its allowed value.

Turning to the  $y$  distributions in Fig. 8, we note that for the  $\nu_e$  reaction (2.7) the  $y$  distribution is flat over nearly the full range (0, 1), rolling off beyond  $y = 0.1$  due to the electron momentum cut (2.8) imposed on the Monte Carlo calculation. The observed  $y$  distribution defined by

$$y_{\text{vis}} = E_{\text{had}} / E_{\text{vis}} \quad (2.11)$$

for the chain reaction (2.4) with an  $8\text{-GeV}/c^2 M^-$  mass is also relatively flat, but for a  $5 \text{ GeV}/c^2 M^-$ , the  $y_{\text{vis}}$  distribution rises rapidly as  $y \rightarrow 1$ . This is especially true with a light-to-heavy quark transition. Hence with a reasonably light  $M^-$  mass, one has the possibility of using the observed  $y$  distributions to discern a heavy-lepton signal from the  $\nu_e$  reaction. \*

In a similar fashion one can use the  $v$  distribution defined by

$$v_{\text{vis}} = x_{\text{vis}} y_{\text{vis}} = E_e (1 - \cos\theta_e) / M \quad (2.12)$$

to distinguish a heavy-lepton signal from background. We illustrate the  $v$  distributions for the three heavy-lepton cases and the  $\nu_e$  reaction in Fig. 9. In the case of reaction (2.7), the  $v$  distribution is broader than that expected for the heavy-lepton process, but it may be difficult to discern the presence of both signals.

Another variable of considerable interest illustrated by Fig. 10 is the transverse momentum for

the electron  $p_{e\perp}$  relative to the incident neutrino beam direction. In the case of the local current transition  $\nu_e \rightarrow e^-$  in (2.7),  $p_{e\perp}$  peaks at zero but can be quite large with a long tail extending up to  $150 \text{ GeV}/c$ . For the nonlocal heavy-lepton reaction,  $p_{e\perp}$  is also peaked at low values ( $1\text{--}2 \text{ GeV}/c$ ) but limited to values less than  $\sim 7.5 \text{ GeV}/c$ . This is one of the most significant differences that we have found.

Two tests which can be used to discriminate between the heavy-lepton process (2.4) and reactions (2.5) and (2.6), where the electron originates at the hadronic vertex, are the distributions in  $z_e = E_e/E_{\text{had}}$  and  $\phi_{e,\text{had}}$ , the opening azimuthal angle between the electron and the hadron-jet direction in a plane perpendicular to the neutrino beam direction. In Fig. 11 we give the  $z_e$  distributions for the electron. In all cases it is peaked near  $z_e = 0$ . For the heavy-lepton reaction (2.4) and the  $\nu_e$  reaction, it extends out beyond  $z_e = 2$  with a long tail up to 10 in most cases. In contrast,  $z_e$  is expected to fall below unity for electrons resulting from semileptonic decays at the hadron vertex. The azimuthal angle  $\phi_{e,\text{had}}$  correlation is shown in Fig. 12 for the heavy-lepton reaction (2.4). In all three cases,  $\phi_{e,\text{had}}$  peaks at  $180^\circ$  but has a long tail extending down to  $0^\circ$ . The  $\nu_e$  reaction yields  $\phi_{e,\text{had}} = 180^\circ$  uniquely, while an electron from the hadronic vertex is expected to peak at  $0^\circ$  with a tail extending toward  $180^\circ$ .

As mentioned earlier, some  $\nu_e$  background is expected in the  $\nu_\mu$  beam at the level of  $\sim 0.5\%$ . Therefore one will have to discriminate a  $\nu_\mu - M^- \rightarrow e^-$  signal from the  $\nu_e \rightarrow e^-$  background.

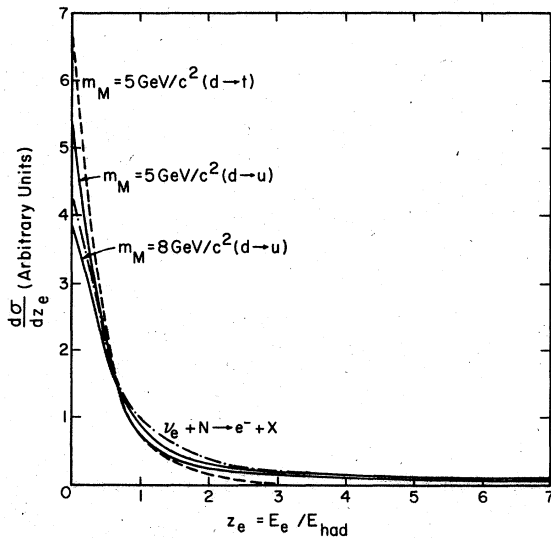


FIG. 11. The distributions in  $z_e = E_e/E_{\text{had}}$ .

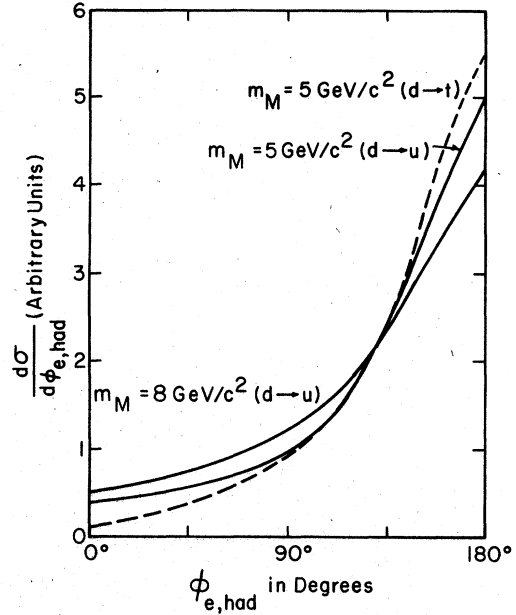
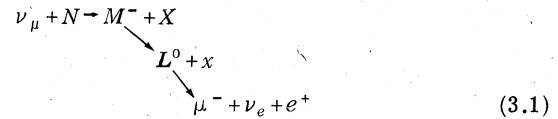


FIG. 12. The distributions in  $\phi_{e,\text{had}}$  the azimuthal angle between the electron and hadronic shower.

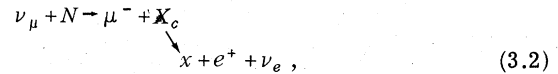
The tests we have proposed above are the most sensitive ones we have found. We have also looked at the opening angle  $\theta_e$  and the rapidity  $Y_e$  but these are not very definitive. In concluding this section, we emphasize that failure to observe a signal from the  $M^-$  chain process in (2.4) does not disprove the existence of an  $M^-$  heavy lepton, but may signify that the  $M^-$  cannot couple directly to the  $e^-$  as required in (2.3).

### III. OPPOSITE-SIGN DILEPTONS: $\mu^- e^+$

In this section we will discuss briefly the chain reaction



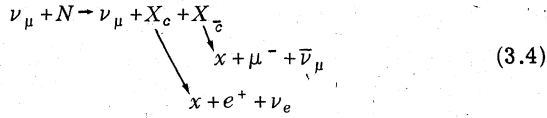
leading to  $\mu^- e^+$  dileptons. Major competition for the reaction comes from the production of charm<sup>8</sup> followed by its semileptonic decay



while other processes include the possible single- $M^0$ -lepton reaction<sup>18</sup>



and associated charm production by the weak neutral current

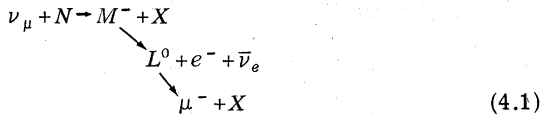


For an 8-GeV/ $c^2$   $M^-$  and a 4-GeV/ $c^2$   $L^0$ , we have previously estimated branching ratios for the  $M^- \rightarrow L^0 + \text{hadron}$  and  $L^0 \rightarrow \mu^- + \nu_e + e^+$  decay modes to be in the ranges of 20–30% and 10–15%, respectively.<sup>19</sup> These numbers enable us to peg the (3.1) chain process at the level of 2–5% of the  $M^-$  production rate given in Sec. II. Taking the production ratios in Table I into account, the estimated rate for (3.1) is found to be in the range 0.02–0.5% of the observed rate for the ordinary  $\nu_\mu + N \rightarrow \mu^- + X$  inclusive reaction. In contrast, one can readily estimate the rate for the chain process (3.2) at the level of ~1–2% of the  $\nu_\mu + N \rightarrow \mu^- + X$  process. The obvious conclusion to be drawn is that the (3.2) chain process will probably overwhelm the heavy-lepton chain reaction (3.1), so this channel is not the best one to look for this signal—except in special kinematical regions.

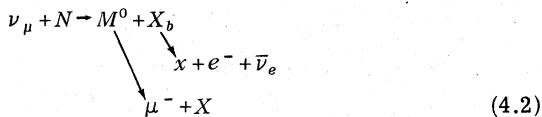
This situation is essentially identical to that encountered in neutrino production of  $\mu^- \mu^+$  dimuons where most of the observed events can be understood in the charm framework.<sup>8</sup> Despite the flux-spectra difference between the double-horn beam used in the bubble-chamber experiments and the quadrupole-triplet beam used in the counter experiments, we find that the flux-averaged distributions for  $\mu^- e^+$  dilepton events occurring through (3.1) are so similar to those presented in Ref. 4 for the  $\mu^- \mu^+$  dimuon events that we do not reproduce them here. We simply note that the best place to maximize the heavy-lepton signal for  $\mu^- e^+$  events relative to the charm process is in the kinematic region where  $E_{\mu^-}/E_{e^+} < 2$ . These so-called “symmetric” dileptons should be quite distinguished from events where the  $e^+$  comes from the hadronic vertex.

#### IV. SAME-SIGN DILEPTONS: $\mu^- e^-$

Turning our attention to the same-sign dilepton processes, we wish to distinguish the heavy-lepton cascade reaction

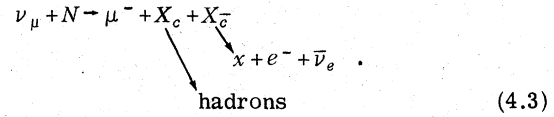


from the single- $M^0$  process<sup>11</sup>



and from associated charm production by the

charged current<sup>10</sup>



Note that the  $\nu_e$  component of the neutrino beam can also induce  $e^- \mu^-$  events via associated charm production, but the expected event rate is negligibly small since the  $\nu_e$  flux relative to the  $\nu_\mu$  flux is less than 1%.

As cited in the Introduction, part of the advantage of studying the same-sign dilepton events in a bubble chamber lies in the fact that for the  $\mu^- e^-$  events, one can hope to decide the leptonic versus hadronic origin of each lepton. (This fact has also been recognized by the authors of Ref. 5, who have independently analyzed the same-sign dilepton reactions.) Hence a study of the  $\mu^- e^-$  events should help to discriminate even better among the reactions (4.1)–(4.3) than one can do in the  $\mu^- \mu^-$  process. The product branching ratio for (3.1) was estimated in Ref. 4 to be 3–7.5%. Together with Table I, this places the  $\mu^- e^-$  production rate at the 0.03–1% level relative to the  $\nu_\mu + N \rightarrow \mu^- + X$  inclusive reaction. Hence of the order 10–200 events would be expected in a 100 000-picture-taking run.

Approximate average values of the energies can be calculated from the following considerations. In reaction (4.1) the  $M^-$  takes approximately  $\frac{2}{3}$  of the total energy and gives  $\frac{1}{3}$  to each lepton (assuming that the  $L^0$  mass is not too large, otherwise it

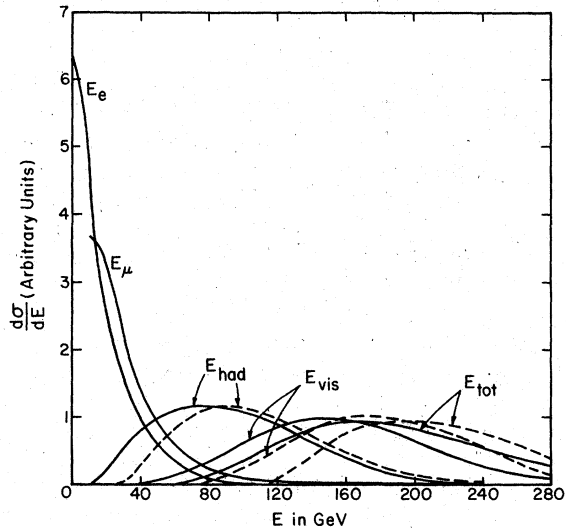
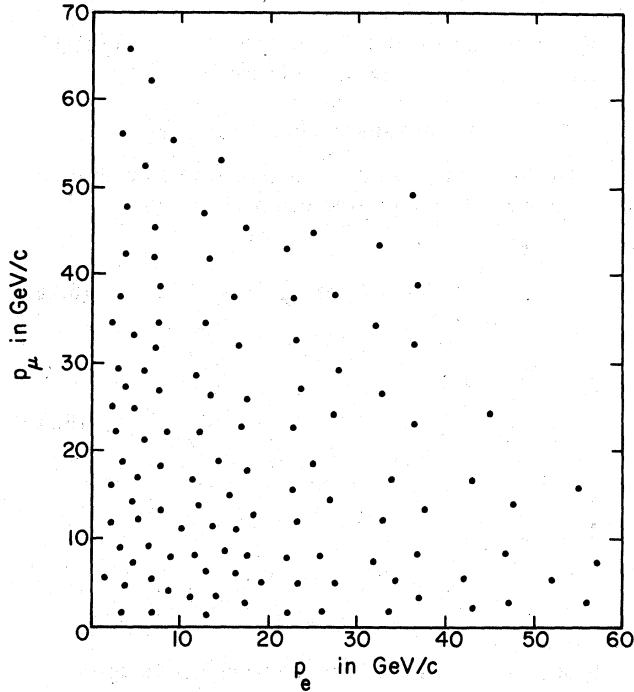


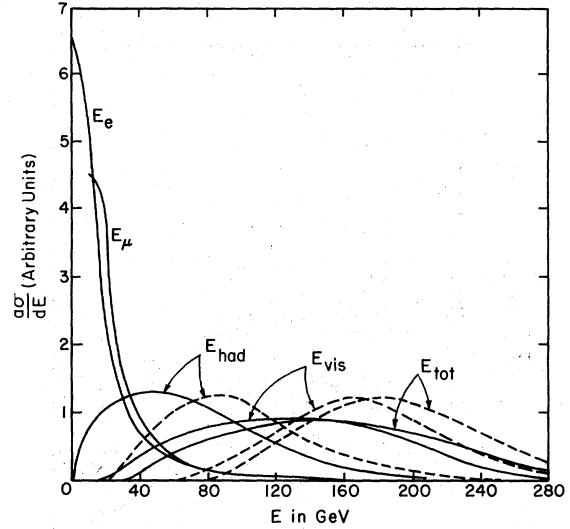
FIG. 13. Energy distributions for the  $e^-$  and  $\mu^-$ , the hadronic energy  $E_{\text{had}}$ , the visible energy  $E_{\text{vis}}$ , and the total energy  $E_{\text{tot}}$ . The solid curves refer to a  $d \rightarrow u$  transition at the hadronic vertex, while the dashed curves refer to a  $d \rightarrow t$  transition.



FIG. 14. Scatter plot of  $p_\mu$  versus  $p_e$ .

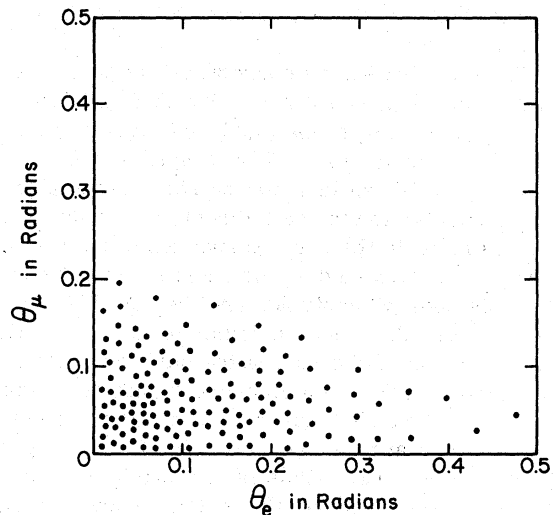
takes more than  $\frac{1}{3}$ ). Hence the average energy of the  $e^-$  is  $\frac{1}{3}$  that of the total while  $\mu^-$  receives  $\geq \frac{1}{3}$ . Actually the  $\mu^-$  receives more energy than the  $e^-$  for  $L^0$  masses in the range 2–4 GeV/ $c^2$ . For the  $M^0$  decay process we expect the  $e^-$  to take  $\sim \frac{1}{18}$  of the average energy while the  $\mu^-$  takes approximately  $\frac{1}{3}$ . This means that  $r = \langle E_{e^-} \rangle / \langle E_{\mu^-} \rangle \sim 1$  for reaction (4.1) and  $r \ll 1$  for reaction (4.2). However, the associated production should also have  $r \ll 1$ , so this does not allow us to distinguish between reactions (4.2) and (4.3).

In Fig. 13, we show the distributions of the electron, muon, hadron, and visible, and total energies for the following choice of parameters:  $m_M = 8$  GeV/ $c^2$ ,  $m_L = 4$  GeV/ $c^2$  and both a  $d \rightarrow u$  and  $d \rightarrow t$  quark transition with  $V-A$  coupling at the hadronic vertex. The hadronic energy distribution at the  $L^0$  decay vertex has been defined in Ref. 4. Comparison of Fig. 13 with Fig. 21 of Ref. 4 reveals that despite the very different flux spectra for the CBF and FHPRW experiments, the hadron, visible and total energy distributions are quite similar. For the parameters chosen, the muon energy distribution is broader than the electron energy distribution. Both the electron and muon energy distributions exhibit greater breadths for the light-to-heavy quark transitions than for the light-to-light transitions since the threshold energy for (4.1) is delayed:  $E_{th} = 90$  GeV compared to 42 GeV. Likewise, as cited in Ref. 4, the  $E_{had}$ ,  $E_{vis}$ , and  $E_{tot}$  distributions are shifted somewhat higher. A scatter plot for the  $p_\mu$  versus  $p_e$  distribution ap-

FIG. 15. Energy distributions for masses  $m_M = 5$  GeV/ $c^2$  and  $m_L = 2$  GeV/ $c^2$  for a  $d \rightarrow u$  transition at the hadronic vertex (solid lines) and a  $d \rightarrow t$  transition (dashed lines). The notation is the same as in Fig. 13.

plicable to the  $d \rightarrow u$  transition is given in Fig. 14. Here again the harder muon spectrum is apparent. By way of contrast, in Fig. 15 we show the same energy distributions for masses  $m_M = 5$  GeV/ $c^2$ ,  $m_L = 2$  GeV/ $c^2$  and both a  $d \rightarrow u$  and  $d \rightarrow t$  quark transition with  $V-A$  coupling. The energies taken by the leptons and hadrons are somewhat lower than in Fig. 13 since the threshold energies are lower:  $E_{th} = 18$  GeV/ $c^2$  for a 5 GeV/ $c^2$   $M^-$  with  $d \rightarrow u$  transition and 53 GeV with a  $d \rightarrow t$  transition.

A scatter plot of  $\theta_\mu$  versus  $\theta_e$  is given in Fig. 16 for the 8-GeV/ $c^2$  and 4-GeV/ $c^2$  mass combination of the heavy leptons and a  $d \rightarrow u$  quark transition.

FIG. 16. Scatter plot of  $\theta_\mu$  versus  $\theta_e$ .

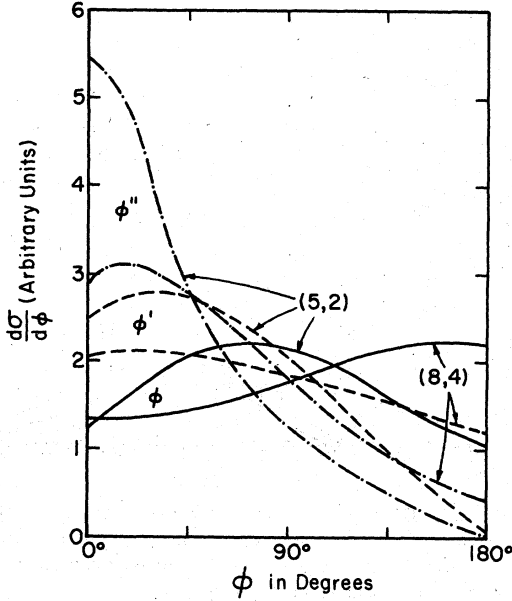


FIG. 17. The spectra in the azimuthal opening angles  $\phi$ ,  $\phi'$ , and  $\phi''$  between the electron and muon vectors.

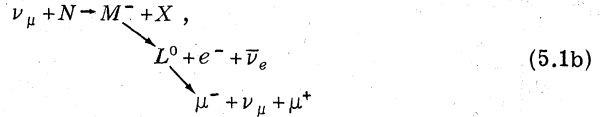
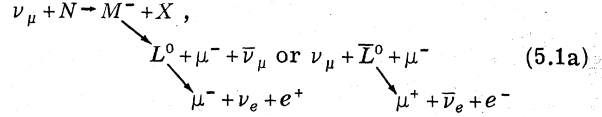
The angles are defined with respect to the beam direction. In this plot it is clear that the (faster on average)  $\mu^-$  tends to come off at a smaller angle with respect to the beam direction than the (slower on average)  $e^-$ . This same correlation was previously observed with respect to the same-sign dimuon events. Similar results were obtained for the other mass values and quark transitions. Likewise, it is found that the rapidity and  $p_{\perp}$  distributions are very similar to those presented in Ref. 4 for the dimuon events, if one identifies the muon and electron with the fast  $\mu^-$  and slow  $\mu^-$ , respectively. The  $x_{vis}$  and  $y_{vis}$  distributions are also similar to those for the dimuon events so we do not repeat them here.

The azimuthal-angle correlations between the muon and electron are presented in Fig. 17 for both mass combinations (8,4)  $\text{GeV}/c^2$  and (5,2)  $\text{GeV}/c^2$  of the  $M^-$  and  $L^0$  heavy leptons with  $d \rightarrow u$  couplings. The solid  $\phi$  curves refer to the plane perpendicular to the beam direction, the dashed  $\phi'$  curves refer to the plane perpendicular to the  $W$  direction determined by the outgoing muon and "visible energy" neutrino, and the dotted  $\phi''$  curves refer to the plane perpendicular to the  $W$  direction defined by using the sum of the muon and electron momenta and the "visible energy" neutrino. Just as in Ref. 4 we find that the azimuthal angle becomes more and more peaked near  $0^\circ$  as one goes from  $\phi$  to  $\phi'$  to  $\phi''$ . This is one of the clearest signals associated with the lepton-cascade phenomena. For an electron coming from the hadronic vertex as in reaction (4.2) or (4.3), one would expect

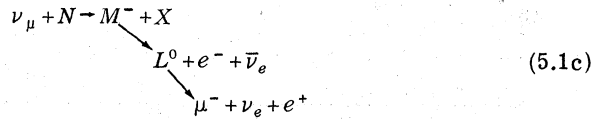
$\phi$  to be peaked at  $180^\circ$ ,  $\phi'$  to be relatively flat, and  $\phi''$  to be slightly peaked near  $0^\circ$ .

#### V. TRILEPTON EVENTS: $\mu\mu e, \mu ee$

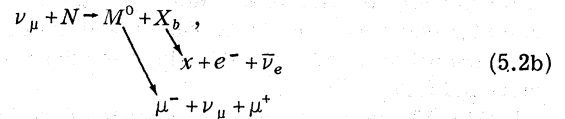
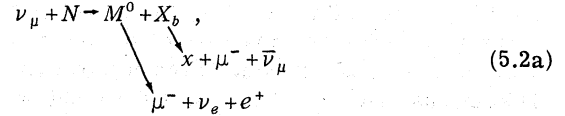
Three classes of trilepton events involving electrons can arise from the chain reactions



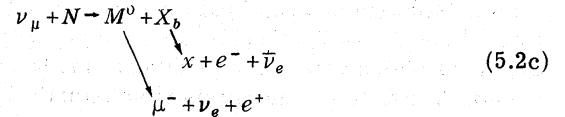
and



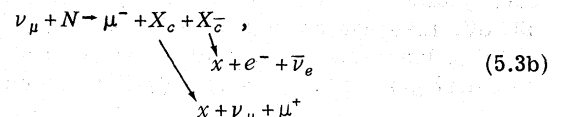
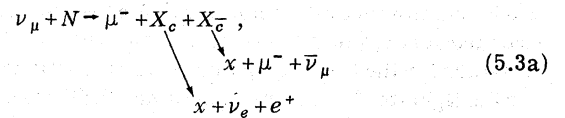
if one considers only charged-current couplings. Tetralepton events can arise if a new quark flavor is produced at the hadron vertex which decays semileptonically into lighter quarks.<sup>20</sup> Possible background reactions for the (5.1) signals involving only one neutral heavy lepton are<sup>11</sup>



and



when the quark transition at the hadron vertex is  $d \rightarrow b$  with the  $b$  flavored object decaying semileptonically. Perhaps the most conventional background arises from charged-current associated charm production<sup>10</sup>:



and

$$\nu_\mu + N \rightarrow \mu^- + X_c + X_{\bar{c}}, \quad (5.3c)$$

where both charmed objects must decay semileptonically.

The event rates for (5.1) have been estimated in Ref. 4 to be at the level of  $(1-20) \times 10^{-4}$  of the single inclusive muon production. Reactions (5.2) and (5.3) would be expected to occur at roughly the same level, so one must distinguish the signals for each reaction by looking at the detailed distributions. In any case, trilepton events are expected to occur rarely in a bubble chamber and to be difficult to identify owing to the great variety of backgrounds. Since one can make use of the distributions presented in Ref. 4 for trimuon events to a good approximation, we shall not present any new figures here. We simply point out that leptons coming from the hadron vertex via charm or other flavor decay should be noticeably softer on the average than those arising from the decay of heavy leptons.

## VI. CONCLUSIONS

We have examined the production of single- $e^-$  and dilepton  $\mu^-e^+$ ,  $\mu^-e^-$  events produced via heavy-lepton decays. These events when identified in a bubble chamber have characteristic distributions which can confirm the heavy-lepton-cascade interpretation of the trimuon events.

The rates for these processes have been calculated by folding in the flux spectrum used by the CBF experiment at Fermilab.<sup>16</sup> Since this spec-

trum is softer than the quadrupole-triplet spectrum used by the FHPRW group,<sup>2</sup> the event rates for the production of a heavy  $M^-$  tend to be rather low.

With a cut on the beam energy of 10 GeV we expect  $\sigma(M^-)/\sigma(\mu^-)$  to be 12% for a 5-GeV/ $c^2$  mass and a regular  $d \rightarrow u$  quark transition. Increasing the mass to 8 GeV/ $c^2$  reduces this number to 3%. The effects due to changing the quark couplings and considering  $d \rightarrow c$  or  $d \rightarrow t$  transitions are given in Table I.

The distributions we have calculated for single  $e^-$  have been compared with electron signals from the background reaction  $\nu_e + N \rightarrow e^- + X$ . Fortunately there are large differences between the spectra so that these processes can be separated. Our distributions for the  $\mu^-e^-$  are very similar to those previously computed for the like-sign  $\mu^-\mu^-$  events, provided we identify the muon with the fast  $\mu^-$  and the electron with the slow  $\mu^-$ . With enough events it should be possible to check our theoretical predictions for the spectra and subject the model to a careful test. We stress the importance of checking the azimuthal correlation between the projected  $e^-$  and  $\mu^-$  vectors on a plane perpendicular to the neutrino beam direction.

The rates for trilepton  $\mu\mu e$  and  $\mu ee$  events are so low that it will be difficult to identify these channels in bubble-chamber experiments owing to the numerous possible backgrounds. We have not given any distributions for these decay modes. We expect them to be very similar to the distributions already presented for the  $\mu^-\mu^-\mu^+$  events.

## ACKNOWLEDGMENT

We wish to thank C. Baltay for informative discussions.

\*Work supported in part by the National Science Foundation under Grants Nos. PHY-75-05476 A 01 and PHY-76-15328.

†Permanent address.

‡Operated by Universities Research Association, Inc., under contract with the U. S. Energy Research and Development Administration.

<sup>1</sup>B. C. Barish *et al.*, Phys. Rev. Lett. **38**, 577 (1977).

<sup>2</sup>A. Benvenuti *et al.*, Phys. Rev. Lett. **39**, 1110 (1977); **39**, 1183 (1977).

<sup>3</sup>M. Holder *et al.*, CERN report (unpublished).

<sup>4</sup>C. H. Albright, J. Smith, and J. A. M. Vermaseren, Phys. Rev. Lett. **38**, 1187 (1977); Phys. Rev. D **16**, 3182 (1977).

<sup>5</sup>V. Barger, T. Gottschalk, D. V. Nanopoulos, J. Abad, and R. J. N. Phillips, Phys. Rev. Lett. **38**, 1190 (1977); see also V. Barger *et al.*, Wisconsin reports and, especially, Phys. Rev. D **16**, 3157 (1977).

<sup>6</sup>B. W. Lee and S. Weinberg, Phys. Rev. Lett. **38**, 1237 (1977); P. Langacker and G. Segrè, Phys. Rev. Lett. **39**, 259 (1977); S. Treiman, F. Wilczek, and A. Zee,

Princeton Univ. report (unpublished).

<sup>7</sup>A. Benvenuti *et al.*, Phys. Rev. Lett. **35**, 1199 (1975); **35**, 1203 (1975); **35**, 1249 (1975); B. C. Barish *et al.*, *ibid.* **36**, 939 (1976).

<sup>8</sup>L. M. Sehgal and P. Zerwas, Phys. Rev. Lett. **36**, 399 (1976); Nucl. Phys. B **108**, 493 (1976); V. Barger and R. J. N. Phillips, Phys. Rev. D **14**, 80 (1976).

<sup>9</sup>This model does not seem to fit the data. See A. Benvenuti *et al.*, Phys. Rev. Lett. **39**, 1183 (1977) and talk by T. Ling at the Washington Meeting of the American Physical Society, 1977 (unpublished).

<sup>10</sup>F. Bletzacker, H.-T. Nieh, and A. Soni, Phys. Rev. Lett. **38**, 1241 (1977); F. Bletzacker and H.-T. Nieh, Stony Brook Report No. ITP-SB-77-42 (unpublished).

<sup>11</sup>R. M. Barnett and L.-N. Chang, Report No. SLAC-PUB-1932, 1977 (unpublished); D. Horn and G. G. Ross, Phys. Lett. **69B**, 364 (1977).

<sup>12</sup>J. Blietschau *et al.*, Phys. Lett. **60B**, 207 (1976).

<sup>13</sup>See article by D. Cline, in *Particles and Fields '76*, proceedings of the Brookhaven meeting of the Division of Particles and Fields of the American Physical So-

- ciety, edited by H. Gordon and R. F. Peierls (BNL, Upton, New York, 1977), p. D37.
- <sup>14</sup>J. P. Berge *et al.*, Phys. Rev. Lett. 38, 266 (1977).
- <sup>15</sup>P. Bosetti *et al.*, Phys. Rev. Lett. 38, 1248 (1977); J. von Krogh *et al.*, *ibid.* 36, 710 (1976).
- <sup>16</sup>C. Baltay *et al.*, Phys. Rev. Lett. 39, 62 (1977).
- <sup>17</sup>The branching ratio for the electron decay mode  $M^- \rightarrow e^- +$  "neutrinos" may be rather large in models which have neutral massive stable leptons. For instance, in the Lee-Weinberg  $SU(3) \times U(1)$  model, the  $M^-$  can decay into both  $e^- E^0 \bar{\nu}_e$ ,  $e^- \bar{E}^0 \nu_\mu$ , and  $e^- E^0 \nu_e \nu_\tau \bar{\nu}_\tau$ . See B. W. Lee and R. E. Shrock, Report No. FERMILAB-Pub-77/48-THY (unpublished).
- <sup>18</sup>L. N. Chang, E. Derman, and J. N. Ng, Phys. Rev. Lett. 35, 6 (1975); Phys. Rev. D 12, 3539 (1975); C. H. Albright, *ibid.* 12, 1319 (1975); A. Soni, *ibid.* 9, 2092 (1974); 11, 624 (1975); A. Pais and S. B. Treiman, Phys. Rev. Lett. 35, 1206 (1975).
- <sup>19</sup>Again we stress that these numbers vary from model to model; see the papers listed in Refs. 5 and 6.
- <sup>20</sup>Tetramuon events arising from the concomitant production of heavy leptons and heavy quarks have been analyzed in detail by C. H. Albright, R. E. Shrock, and J. Smith [Report No. FERMILAB-Pub-77/81-THY (unpublished)]. Note that such events can be produced in a pure leptonic cascade if the mass of the  $L^0$  is light enough so that the decay  $M^- \rightarrow L^0 \bar{L}^0 + X$  is allowed.